AIP | Journal of Applied Physics

Structure, electrical and magnetic property investigations on dense Fe-doped hexagonal BaTiO3

X. K. Wei, Y. T. Su, Y. Sui, Q. H. Zhang, Y. Yao et al.

Citation: J. Appl. Phys. **110**, 114112 (2011); doi: 10.1063/1.3658813
View online: http://dx.doi.org/10.1063/1.3658813
View Table of Contents: http://jap.aip.org/resource/1/JAPIAU/v110/i11
Published by the American Institute of Physics.

Structure, electrical and magnetic property investigations on dense Fe-doped hexagonal $BaTiO_3$

X. K. Wei,[1] Y. T. Su,[2] Y. Sui,[2] Q. H. Zhang,[1] Y. Yao,[1] C. Q. Jin,[1] and R. C. Yu[1,a)]
[1]*Beijing National Laboratory for Condensed Matter Physics, Institute of Physics, Chinese Academy of Sciences, Beijing 100190, People's Republic of China*
[2]*Center for Condensed Matter Science and Technology, Department of Physics, Harbin Institute of Technology, Harbin 150001, People's Republic of China*

(Received 24 August 2011; accepted 3 October 2011; published online 6 December 2011)

Hexagonal $Ba(Ti_{1-x}Fe_x)O_{3-\delta}$ ($x = 1/6$, 1/3) ceramics treated with post annealing are specifically synthesized to explore the origin mechanism of the unusual ferromagnetism in the doped system. X-ray diffraction refinements and transmission electron microscope experiments reveal that their structures are incommensurately modulated owing to simultaneous oxygen vacancies at both O1 and O2 sites. Consequently, coexisting weak ferrielectricity and weak ferromagnetism are presented at room temperature. Analysis on their leakage current plot reveals that their conduction follows trap-filled limit model. In combination with the magnetism studies on 5 mol% Fe-doped crystals [Phys. Rev. B **83**, 144407 (2011)], the reduction of ferromagnetism with an increase of conductivity suggests that dynamic exchanges of trapped electrons among the bound magnetic polarons attribute to the intrinsic ferromagnetism. © *2011 American Institute of Physics*. [doi:10.1063/1.3658813]

I. INTRODUCTION

$BaTiO_3$ based materials are of fundamental importance due to their widespread technological applications in capacitors, positive temperature coefficient of resistance thermistors, etc.[1] Triggered by integrating multiple functionalities in one material, alternation of physical properties through compositional modification has been widely carried out in perovskite $BaTiO_3$ and coexistence of ferromagnetism (FM) and ferroelectricity at room temperature were reported.[2–4] As another polymorph of $BaTiO_3$, hexagonal (6H) $BaTiO_3$ has increasingly attracted the attention recently because of its unusual high-temperature FM caused by magnetic Fe ion doping of B-site Ti,[5,6] especially when the doping concentration is less than 10 mol%.[7,8] Subsequently, the origin of the FM in the dilute magnetic oxide becomes controversial owing to the possible dopant clustering and precipitation of secondary magnetic phase responsible for the possible extrinsic signals. However, some convincing experimental results have pointed out that the magnetism is intrinsic and is induced by oxygen vacancies (Vos).[5,8]

To figure out the magnetism origin in the doped system, different approaches can be implemented. As Chakraborty *et al*. reported in Ref. 8, samples with consistent dilute Fe doping but different vacancy deficiency have been used, accordingly, their magnetic and electrical property changes as a function of the vacancy content can provide substantial evidences. Considering the doping limit of Fe in this hexagonal matrix, which ranges from ~1 mol% to 67 mol% or even higher,[1,7,9] samples with doping content slightly higher than 10 mol% are also good candidates for the mechanism exploration because of the exclusion to the extrinsic factors. Meanwhile, it is also interesting to investigate the multiferroic behaviors in the hexagonal matrix. To be noted, relative to dilute Fe-doped samples with less vacancy deficiency, the electrical property of densely doped samples may be more conductive owing to more dopant and vacancies.[10]

In this paper, we report the magnetic and electrical properties of post-annealed (PA) 6H-$Ba(Ti_{1-x}Fe_x)O_{3-\delta}$ ($x = 1/6$, 1/3) based on detailed structure investigations. In combination with the refinement results of X-ray diffraction (XRD), transmission electron microscope (TEM) experiments reveal that Vos at both O1 and O2 sites result in incommensurate structure modulations. Consequently, the FM at room temperature is weakened by one order of magnitude due to the complex defect structures. However, lattice translational symmetry breaking leads to the simultaneous appearance of weak ferrielectricity at room temperature. Through analyzing the susceptibility, current leaking curves, and dielectric behaviors, our experimental results point out that the density ratio between trapped electrons and mobile carriers fundamentally determines the ferromagnetic exchange of the doped system around room temperature.

II. EXPERIMENTS

Using stoichiometric amounts of $BaCO_3$, TiO_2, and Fe_2O_3, polycrystalline $Ba(Ti_{1-x}Fe_x)O_{3-\delta}$ ($x = 1/6$ and 1/3) samples (short for BTF17 and BTF33 hereafter) prepared with solid state reaction method were PA in air at 1100 °C for 20 h.[11] The XRD was performed on Philips X'Pert Pro powder diffractometer (Cu $K\alpha_1$ $\lambda = 1.5406$ Å) with a scan step of 0.017 ° and the data pattern was refined using FULLPROF software package. The TEM specimen was prepared by crushing the sample in ethanol and then supporting the fragments on the carbon-film coated cooper grid. Our TEM

a)Author to whom correspondence should be addressed. Electronic mail: rcyu@aphy.iphy.ac.cn.

observations performed on FEI Tecnai F20 reveal that there are no dopant clustering and secondary phases in the doped system. DC magnetic measurements were performed on Quantum Design Physical Property Measurement System (PPMS). The susceptibility data were collected in the warming cycle for the zero-field-cooling mode and cooling cycle for the field-cooling modes, respectively, no divergence was observed. Temperature dependence of dielectric constant (ε_r) and loss tangent ($\tan\delta$) are measured on a Hewlett-Packard 4192A gain phase analyzer and silver paste was painted on sample surface as electrode. The scanning frequency ranges from 1 kHz to 100 kHz and the temperature accuracy for the measurements (from 213 K to 453 K) is $\Delta T = \pm 1$ K. The room temperature ferroelectric loops (P vs E), switching current (I vs E), and leakage current (J vs E) curves were measured on TF 2000 FE analyzer.

III. RESULTS AND DISCUSSION

A. Structural investigation

Figure 1 shows the refined XRD patterns of PA BTF17 and PA BTF33 using the space group of $P6_3/mmc$ of 6H-$BaTiO_3$. As verified by the structural investigations on as-grown BTF17 which is structural phase separated,[11] simultaneous presence of vacancies at O1 and O2 sites in PA BTF17 and PA BTF33 is obtained in our refinements, and this is different from the common condition that vacancies occupy the O1 site only[5,9,12–15] as the doping content is less than $x = 0.67$ or the vacancy content is less than $\delta = 0.32$. According to our TEM observations (see below), defect structures caused by O1 and O2 vacancies may attribute to the unfavorable refinement factors, $R_p/R_{wp} = 14.1/12.7$ and 14.4/11.9 for PA BTF17 and PA BTF33, respectively.

Figs. 2(a)–2(c) show the electron diffraction (ED) patterns of PA BTF17 taken along different zone axes, the satellite diffraction spots appeared around the fundamental spots reveal that PA BTF17 is of purely incommensurately modulated. The ED pattern taken along [0001] zone axis (Fig. 2(a)) reveals that the satellite spots without accurately locating in (0001)* plane show splitting characters and form

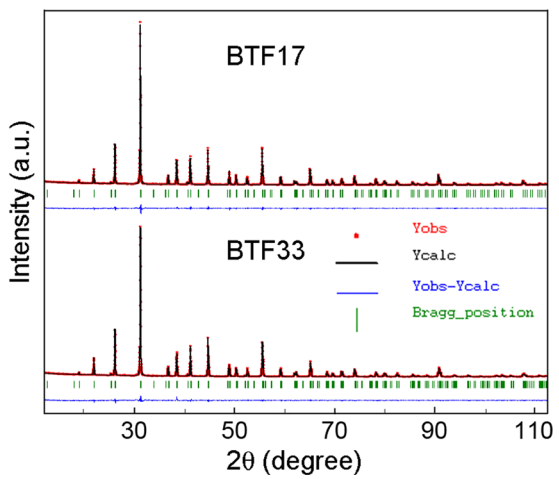

FIG. 1. (Color online). The refined XRD patterns of PA BTF17 and PA BTF33 at room temperature.

an angle of $\phi \approx 25.6°$ relative to $\mathbf{g}_{(1120)}$ reciprocal vector. Along $[4\bar{2}\bar{2}3]$ and $[22\bar{4}3]$ zone axes, more asymmetric projections of the satellite spots are observed. However, modulation reflections do not exist along $\langle 01\bar{1}0\rangle$ directions (Figs. 2(b), 2(c), and 2(f)). These results indicate that the displacement of atoms takes place mainly in *a,b*-plane and formation of dislocations results in the structural modulations, which can be identified from the high-resolution TEM (HRTEM) images. For example along [0001] zone axis, the satellite spots yield an average modulation wavelength of $2\lambda \approx 2.94$ nm; the modulated wide and narrow stripes (~6 nm and ~1.5 nm in width, respectively) correspond to the different modulated reflections and the angle between the two types of domains attribute to the splitting of the satellite spots (Fig. 2(d)). Meanwhile, antiphase domain boundaries caused by defect structures can be identified from the inversed filtered-Fourier-transformation (IFFT) images in the inserts of Figs. 2(d) and 2(e).

For PA BTF33, the modulation characters change evidently. In Fig. 3(a), the [0001] ED pattern reveals that the satellite spots indicated by $\boldsymbol{q}_1$ and $\boldsymbol{q}_2$ exhibit a larger splitting angle, $\beta \approx 26°$. Correspondingly, their average modulation wavelength is $2\lambda \approx 3.06$ nm and as Fig. 3(d) shows, the competing antiphase domains ranging from ~4 nm to ~10 nm become more equivalent. Besides the modulation reflections along $[4\bar{2}\bar{2}3]$ zone axis, asymmetric modulation reflections appear along $[1\bar{1}0\bar{1}]$ zone axis (see Figs. 3(b) and 3(c)). Similarly, the incommensurate modulations are not observed along $\langle 01\bar{1}0\rangle$ zone axis (see Fig. 3(f)). These structural features suggest that lattice translational symmetry is broken due to the defect structures caused by O1 and O2 vacancies.

B. Electrical properties

Figure 4(a) shows the leakage log$J$ vs V plots of PA BTF17 and PA BTF33. These two curves show symmetric characteristics thus we can rule out the interface-limited conduction.[16] As the doping concentration increases from 1/6 to 1/3, the leakage current density increases by two orders of magnitude. For better understanding the conduction mechanism, the log$J$ vs V plot is presented on a double logarithmic scale. As Fig. 4(b) shows, the log$J$ vs log$V$ curves well follow linear behaviors and their slope α obtained by linear fitting is 1.12 and 1.16, respectively. According to Lampert' theory,[17,18] the log$J$ vs log$V$ plot with a constant slope of $1 < \alpha < 2$ indicates that the conduction mechanism of the two samples is ascribed to the trap-filled limit model.

When B-site Ti^{4+} ions are partially replaced by Fe^{3+}, some impurity states are created by the accompanied Vos within the band gap,[19] and they act as trap levels to capture the injected electrons inside the sample. In real samples, shallow (above the Fermi level) and deep (below the Fermi level) traps distribute over several energy states and correspondingly different activation energies are required to excite the trapped electrons to the conduction level.[17] When the deep traps are completely filled up at a critical voltage, i.e., the trap-filled limit voltage (V_{TFL}), no more injected electrons are trapped in the deep trap levels at further fields. Beyond V_{TFL}, all injected electrons at that field thus take part

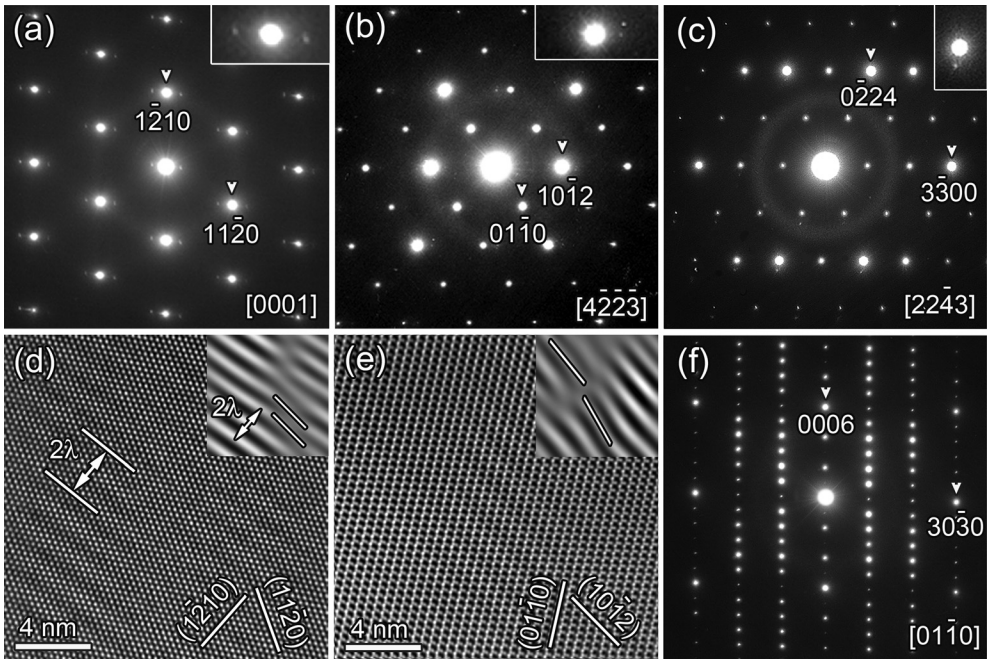

FIG. 2. (a)-(c) The ED patterns of PA BTF17 taken along [0001], $[4\bar{2}\bar{2}\bar{3}]$, and $[22\bar{4}3]$ axes, respectively, and the inserts are the enlarged typical reflections. (d) and (e) The corresponding HRTEM images of (a) and (b), respectively, and the inserts are the inversed filtered Fourier transformation (IFFT) images (with the same magnification) obtained from the satellite spots around the transmitted spot, respectively. The modulation wavelength 2λ comes from the stronger satellite spot. (f) The ED pattern taken along $[01\bar{1}0]$ zone axis.

in the conduction and a sudden jump in the current can be observed.[17] The dielectric measurements provide further verification.

Temperature dependence of ε_r and $\tan\delta$ of PA BTF17 is shown in Fig. 5(a), and strong frequency dispersion at the higher temperature region can be observed. Meanwhile, the ferroelectric measurements reveal that the doped sample has weak ferrielectricity at room temperature. In spite that the dielectric behaviors resemble to that in high-dielectric-constant $CaCu_3Ti_4O_{12}$ (Ref. 20) or relaxor ferroelectrics $Pb(Mg_{1/3}Nb_{2/3})O_3$,[21] the dielectric relaxation caused by Maxwell-Wagner effect cannot be concluded here because of our limited temperature range. However, the origin of the dielectric relaxation can be more clearly figured out in highly doped PA BTF33.

Figures 6(a) and 6(b) show the temperature dependent ε_r and $\tan\delta$ of PA BTF33, and similarly, strong dielectric relaxation is observed. Because of the large leakage current, dielectric breakdown[22] comes into being from about 360 K as the measurement frequency increases from $f = 1$ kHz to higher. Correspondingly, the dielectric loss increases steeply. When plotting the relationship between f_r and temperature (T) extracted from the maximum of $\tan\delta$ (see the insert of Fig. 6(b)), we find that the linear relation can be best fitted by the Arrhenius model,

$$f_r = f_0 \exp(-E_a/k_B T), \tag{1}$$

wherein, k_B is the Boltzman constant. The relaxation frequency at an infinite temperature is $f_0 = 1.37 \times 10^{10}$ Hz

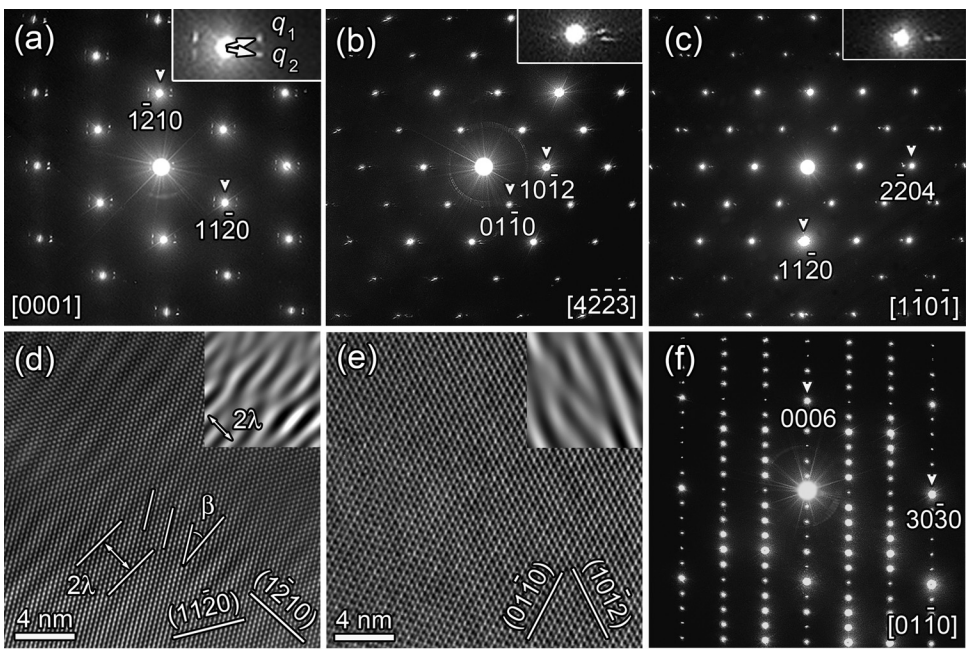

FIG. 3. (a)-(c) The ED patterns of PA BTF33 taken along [0001], $[4\bar{2}\bar{2}\bar{3}]$,and $[1\bar{1}0\bar{1}]$ axes, respectively, and the inserts are the enlarged typical reflections. (d) and (e) The corresponding HRTEM images of (a) and (b), respectively, and the inserts are the IFFT images (with the same magnification) obtained from the satellite spots around the transmitted spot, respectively. The modulation wavelength 2λ comes from q_2. (f) The ED pattern taken along $[01\bar{1}0]$ zone axis.

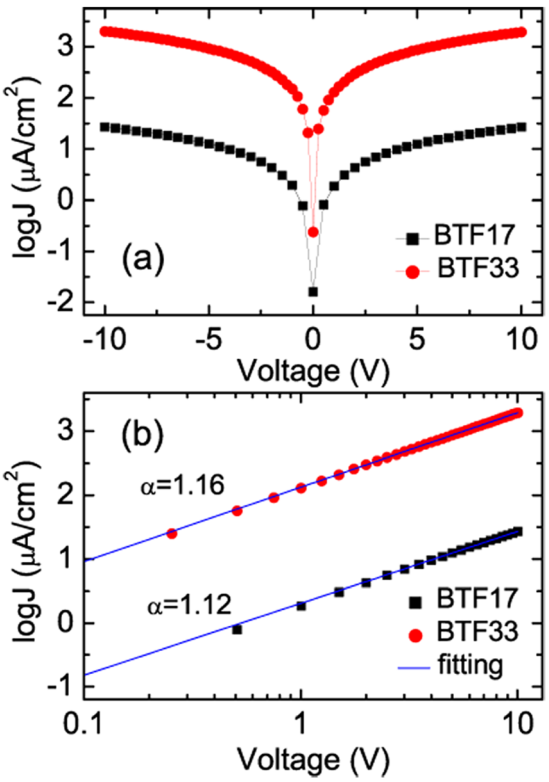

FIG. 4. (Color online) (a) The log$J$ vs E and (b) log$J$ vs log$E$ plots of PA BTF17 and PA BTF33 measured at room temperature. The lines are the fitted results.

(relaxation time $\tau_0 = 1.16 \times 10^{-11}$ s) and the activation energy for the relaxation is $E_a = 0.38$ eV (the insert of Fig. 6(b)). Considering the activation energy for ion jumping (0.2 eV-1 eV),[23] these results suggest that the dielectric

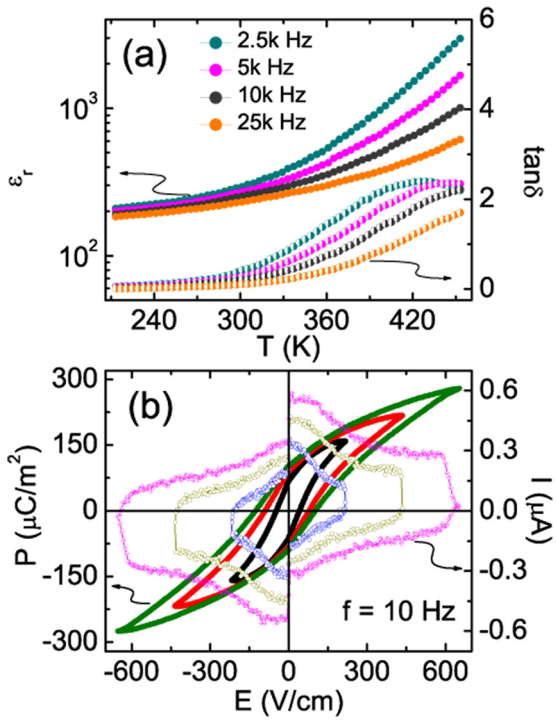

FIG. 5. (Color online) (a) The temperature dependences of ε_r and tan δ of PA BTF17. (b) The ferroelectric loops and switching current of PA BTF17 measured at $f = 10$ Hz and room temperature.

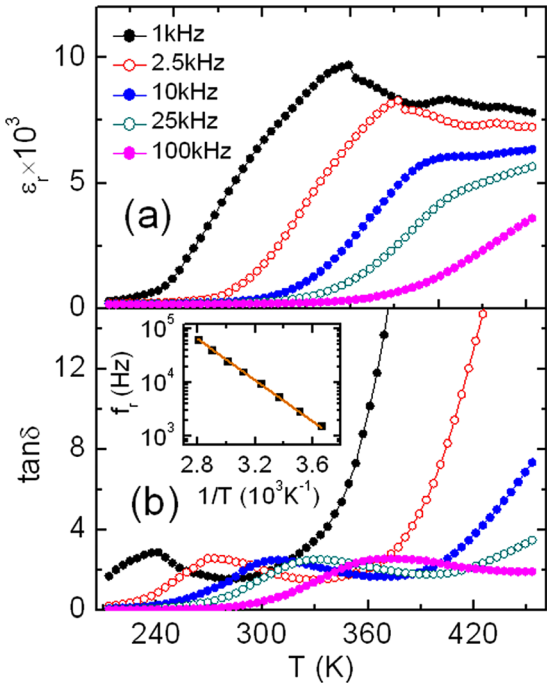

FIG. 6. (Color online) (a) and (b) Temperature dependences of ε_r and tanδ of PA BTF33. The insert of (b) is the plot of logf_r vs $1/T$ fitted with the Arrhenius relation.

relaxation in PA BTF17 and PA BTF33 may attribute to motion of Vos and related defects aided by thermally excited detrapping electrons and polarons.[10,17,22] From structure point of view, the relaxation can be ascribed to the polarized nanodomains caused by the defect structures in the sample.

The ferroelectric measurements reveal that PA BTF33 exhibits dynamic ferrielectric transitions at room temperature. In Fig. 7(a), a ferrielectric state which is very close to an antiferroelectric state is observed at $f = 100$ Hz. However, when frequency increases to $f = 500$ Hz and above, ferrielectric states prone to ferroelectric loops are presented (Figs. 7(b)–7(d)). When viewing the concomitant switching current plots, the sudden changes of I at the maximum of E suggest that the ferrielectric transition is possibly achieved

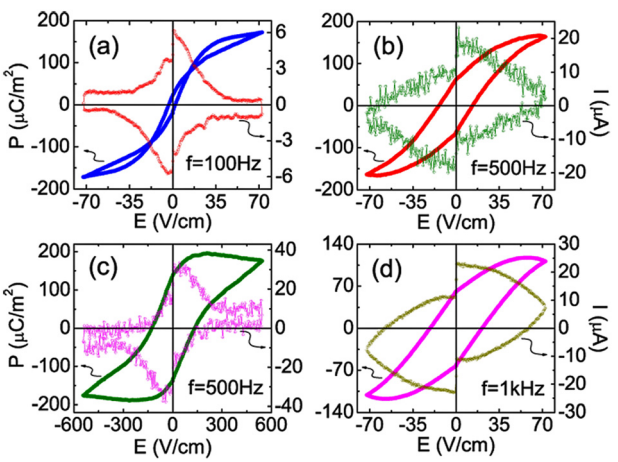

FIG. 7. (Color online) The P vs E and I vs E plots of PA BTF33 measured at (a) $f = 100$ Hz, (b) and (c) $f = 500$ Hz, and (d) $f = 1$ kHz at room temperature.

through the motion of charged Vos. For PA BTF17, the wide modulated stripes outweigh the narrow ones, thus the ferrielectric loops show weak frequency dependence. However, for PA BTF33, counterbalanced nanodomains, as indicated by $\boldsymbol{q}_1$ and $\boldsymbol{q}_2$ with equivalent reflection intensities and large splitting angle, result in an evident ferrielectric transition. For the magnitude of the polarization $\sim 10^2\ \mu C/m^2$, this may be ascribed to the destruction of the defect structures to the centrosymmetric hexagonal $BaTiO_3$ matrix.

C. Magnetic properties

For PA BTF17 and PA BTF33, their magnetic properties resemble to that of dilute Fe-doped samples.[7,8] As Fig. 8(a) shows, their susceptibilities (χ) also show concave temperature dependences, and the hysteresis loops measured at 5 K and 300 K are of paramagnetic and ferromagnetic, respectively. Meanwhile, the magnetization decreases with the increasing doping of magnetic Fe, and this is consistent with the result reported by Lin *et al.*[5] If we compare with the dilute doped samples,[7,8] the magnetization reduces by one order of magnitude (see Figs. 8(b) and 8(c)), this weakening may fundamentally be caused by the destruction of perfect crystal structure due to Vos. Meanwhile, the $1/\chi$ within an interval from 130 K to 300 K follows a good linear dependence on temperature. However, Curie-Weiss law is still not applicable for the linear part around room temperature because of the room-temperature FM.

D. Discussion

In our experiments, the doping concentrations of $x = 1/6$ and 1/3 are chosen according to the B-site occupation ratio between the two un-equivalent atomic sites of M1 and M2, i.e., $M2/(M1 + M2) = 2/3$, and the post annealing treatment

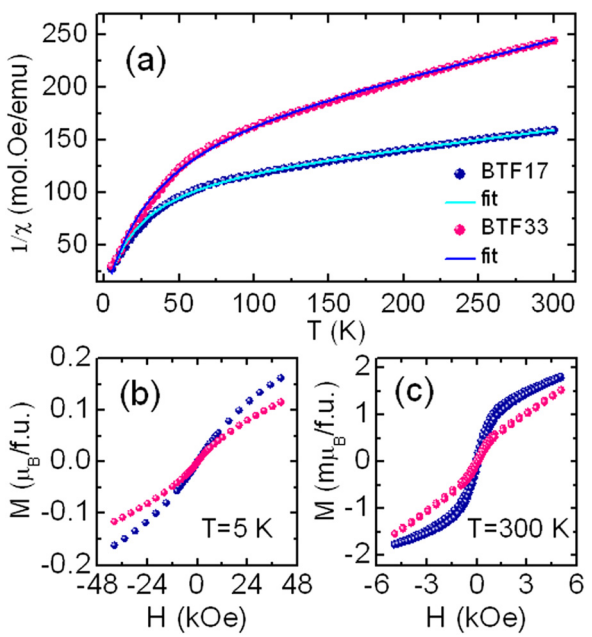

FIG. 8. (Color online) (a) Temperature dependence of $1/\chi$ of PA BTF17 and PA BTF33 measured at $H = 500$ Oe. (b) and (c) The magnetic hysteresis loops of the two samples measured at 5 K and 300 K, respectively.

is expected to decrease the vacancy content and enhance the magnetization.[24] Consistent with the previous reports,[5,8] our results also agree with the conclusion that FM in this doped system is induced by Vos. However, in our experiments, the relationship between magnetism and current leaking behaviors in PA BTF17 and PA BTF33 reveal that the sample conductivity caused by the dopant and Vos plays a crucial role in producing the FM. Comparison of the dilute doped samples treated under different conditions,[8] the charge carrier density in the sample annealed at higher vacuum condition should be larger than the other two. Accordingly, the larger is the conductivity, the stronger is the FM. However, as verified by our results and that of Lin *et al.*,[5] more mobile charge carriers coming from the Fe^{3+} ions and the electrons compensating the Vos reduce the FM of the doped system greatly. Therefore, the density ratio between mobile charge carriers and trapped electrons should be a crucial parameter in determining the origin of FM in the doped system. To be noted is that this conclusion excludes the presence of Fe^{4+} ions.[24]

Therefore, through reviewing the magnetic behaviors of the doped system,[5,7,8] the contrast between room-temperature FM and ground-state paramagnetism suggests that the origin of the FM correlates intimately with the hopping of trapped electrons, which shows strongly thermal dependence. Through fitting the susceptibility curves, we find that a limited polynomial expression can give a best fitting

$$\chi = p_1(H)T^{-1} + p_2(H) + p_3(H)T. \quad (2)$$

The strong dependences of χ on T and H indicate that the unusual FM is derived from a dynamical nature. The $p_1(H)T^{-1}$ item attributes to the ground state paramagnetism; while the rest items account for the FM in the temperature region beyond the ground state, in which the contribution from the linear item may possibly be responsible for the excitation of trapped electrons from the impurity band (see Table I). Referring to the defect-driven mechanism in systems such as dilute magnetic semiconductors (DMS),[25] therefore, the unusual FM in Fe-doped hexagonal $BaTiO_3$ may be caused by dynamic exchanges of trapped electrons among the bound magnetic polarons.

Assuming all Fe^{3+} ions adopt the low-spin arrangements at M2 site, which is consistent with the first-principles calculations on dilute Fe-doped $BaTiO_3$ crystals,[7] the calculation according to the paramagnetic Curie parameter $p_1(H)$ yields that about 26% and 13% Ti^{4+} ions are reduced to Ti^{3+} in PA BTF17 and PA BTF33, respectively. The calculated results may not be the real content of Ti^{3+} ions since the doped Fe^{3+} ions do not fully occupy at M2 site, but the presence of

TABLE I. The fitted parameters using the limited polynomial expression.

X	$p_1(H)$	$p_2(H)/10^{-3}$	$P_3(H)/10^{-5}$
1/6	0.17343	7.33	−5.50
1/3	0.18739	4.70	−4.18

Note: The units of $p_1(H)$, $p_2(H)$, and $p_3(H)$ are emu K mol^{-1} Oe^{-1}, emu mol^{-1} Oe^{-1}, and emu K^{-1} mol^{-1} Oe^{-1}, respectively.

Ti^{3+} ions and their contribution to the magnetic and electrical properties are not negligible, as reported by Chakraborty *et al*. in 5 mol% Fe-doped crystals.[8]

IV. CONCLUSIONS

In conclusion, X-ray diffraction refinements and transmission electron microscope investigations on post-annealed hexagonal $Ba(Ti_{1-x}Fe_x)O_{3-\delta}$ ($x = 1/6$ and $1/3$) reveal that owing to the defect structures introduced by oxygen vacancies at both O1 and O2 sites, their structures show incommensurate modulation features. Symmetry breaking of lattice translation results in the coexistence of weak ferrielectricity and ferromagnetism at room temperature. Analysis on the leakage current plots reveals that the conductivity of the samples follows trap-filled limit model. Consequently, thermal excitation to the trapped electrons results in the dielectric breakdown above room temperature, as observed in PA BTF33. According to the results reported on dilute Fe-doped $BaTiO_3$ crystals,[8] our experimental results suggest that dynamic exchanges of trapped electrons among bound magnetic polarons attribute to the ferromagnetism at ambient temperature.

ACKNOWLEDGMENTS

This work was supported by the National Natural Science Foundation of China (Grant Nos. 11174336 and 50921091) and the specific funding of Discipline and Graduate Education Project of Beijing Municipal Commission of Education.

[1]G. M. Keith, M. J. Rampling, K. Sarma, N. M. Alford, and D. C. Sinclair, J. Eur. Ceram. Soc. **24**, 1721 (2004).
[2]B. Xu, K. Yin, J. Lin, Y. Xia, X. Wan, J. Yin, X. Bai, J. Du, and Z. Liu, Phys. Rev. B **79**, 134109 (2009).
[3]R. Maier, J. L. Cohn, J. J. Neumeier, and L. A. Bendersky, Appl. Phys. Lett. **78**, 2536 (2001).
[4]Y. H. Lin, J. C. Yuan, S. Y. Zhang, Y. Zhang, J. Liu, Y. Wang, and C. W. Nan, Appl. Phys. Lett. **95**, 033105 (2009).
[5]F. Lin, D. Jiang, X. Ma, and W. Shi, J. Magn. Magn. Mater. **320**, 691 (2008).
[6]F. Lin and W. Shi, J. Alloys Compd. **475**, 64 (2009).
[7]S. Ray, P. Mahadevan, S. Mandal, S. Krishnakumar, C. Kuroda, T. Sasaki, T. Taniyama, and M. Itoh, Phys. Rev. B **77**, 104416 (2008).
[8]T. Chakraborty, S. Ray, and M. Itoh, Phys. Rev. B **83**, 144407 (2011).
[9]I. E. Grey, L. Christina, L. M. D. Cranswick, R. S. Roth, and T. A. Vanderah, J. Solid State Chem. **135**, 312 (1998).
[10]E. Mashkina, Ph.D. dissertation, Naturwissenschaftlichen Fakultäten der Friedrich-Alexander-Universität, 2005.
[11]X. K. Wei, Q. H. Zhang, F. Y. Li, C. Q. Jin, and R. C. Yu, J. Alloys Compd. **508**, 486 (2010).
[12]E. Mashkina, C. McCammon, and F. A. Seifert, J. Solid State Chem. **177**, 262 (2004).
[13]I. E. Grey, L. M. D. Cranswick, and C. Li, J. Appl. Cryst. **31**, 692 (1998).
[14]T. Colson, M. Spencer, and I. Yarovsky, Comput. Mater. Sci. **34**, 157 (2005).
[15]A. J. Jacobson, Acta Cryst. B **32**, 1087 (1976).
[16]Y. Shuai, S. Zhou, D. Buürger, H. Reuther, I. Skorupa, V. John, M. Helm, and H. Schmidt, J. Appl. Phys. **109**, 084105 (2011).
[17]A. R. Chaudhuri and S. B. Krupanidhi, J. Appl. Phys. **98**, 094112 (2005).
[18]M. A. Lampert and P. Mark, *Current Injection in Solids* (Academic, New York, 1970).
[19]Y. Akishige, Y. Yamazaki, and N. Môri, J. Phys. Soc. Jpn. **73**, 1267 (2004).
[20]C. C. Homes, T. Vogt, S. M. Shapiro, S. Wakimoto, and A. P. Ramirez, Science **293**, 673 (2001).
[21]S. Kamba, M. Kempa, V. Bovtun, J. Petzelt, K. Brinkman, and N. Setter, J. Phys.: Condens. Matter **17**, 3965 (2005).
[22]R. Waser, T. Baiatu, and K.-H. Härdtl, J. Am. Ceram. Soc. **73**, 1645 (1990).
[23]L. Zhang and Z. J. Tang, Phys. Rev. B **70**, 174306 (2004).
[24]F. Lin, D. Jiang, X. Ma, and W. Shi, Physica B **403**, 2525 (2008).
[25]J. M. D. Coey, M. Venkatesan, and C. B. Fitzgerald, Nat. Mater. **4**, 173 (2005).